J. Water Environ. Nanotechnol., 4(1): 75-87 Winter 2019

ORIGINAL RESEARCH PAPER

Environmental impacts related to MWCNT-COOHs, TiO_2 and NM nanoparticles on the cement composites with quality factor and RSM concept

Ali Bahari*, Mohammad Ali Mousavi, Hosein Milani Moghadam

Department of solid state Physics, University of Mazandaran, Babolsar, Iran

Received: 2018-08-27 Accepted: 2018-10-01 Published: 2019-02-01

ABSTRACT

The use of nanotechnology in replacing cement with nanomaterials due to environmental aspects and reduction of pollutants is presently an important issue in the world.

In this regard, the effect of various weight percentages of functionalized carbon nanotubes together with montmorillonite nanoparticles and with titanium oxide nanoparticles were studied as replacements for the cement to improve the mechanical and microstructural properties of hardened cement paste composites. In the present study, carbon nanotubes, TiO_2, and montmorillonite nanoparticles were synthesized as additions into cement matrix, and their nano-structural characterizations were studied using the TEM, XRD, X-Powder, DSC-TGA, FTIR, and GPS132A techniques. The obtained results indicate that the addition of nanomaterials to cement-based composites improves mechanical, electrical and nano-structural properties and the quality as well as emission factors of samples with optimization portion of nano-particles found by RSM method.

Keywords: *CVD; WCNT; Nanomaterials; Nano-montmorillonite (NM); Portland cement (PC); Quality factor (Q_F); Response surface methodology (RSM); TiO_2*

How to cite this article

Bahari A, Mousavi MA, Milani Moghadam H. Environmental impacts related to MWCNT-COOHs, TiO_2 and NM nanoparticles on the cement composites with quality factor and RSM concept. J. Water Environ. Nanotechnol., 2019; 4(1): 75-87. DOI: 10.22090/jwent.2019.01.008

INTRODUCTION

Portland cement-based materials such as concrete and mortar are widely used in building materials in today's world and are mostly applied in the construction industry [1]. Nearly 4 billion tons of these materials were produced in 2011 [2]. The cement industry is currently generating about 8% of global greenhouse gas emissions, such as CO_2. While global cement production is expected to increase it by more than 4 billion tons due to an increase in demand for housing and infrastructure projects as shown in Fig. 1 [3-5]. Along with global policies to achieve sustainable development, many efforts have been made to reduce emissions of pollutants such as the use of replacing materials that reduce cement consumption [6]. Although some researchers have reported that increased cement consumption in cement-based products will improve mechanical properties, it is scientifically unacceptable. What is confirmed by the construction industry researchers is achieving an optimal percentage? On the other hand, for sustainable development and environmental protection, it is necessary to reduce cement consumption or at least not to increase it [7-10]. So, the use of nano-scale materials due to their unique characteristics and their performance differences over larger materials can be a good alternative to cement replacement, resulting in a significant reduction in its use [11-17]. Many researchers have made fundamental changes in science in recent years, utilizing nanotechnology and the use of various nanomaterials [18-22]. Among the most widely used nano-materials, there are carbon nanotubes (CNT), nano-titanium oxide or titanium (TiO_2) and nano-

* Corresponding Author Email: *a.bahari@umz.ac.ir*

montmorillonite (NM). The preferred mechanical properties of carbon nanotubes have introduced this nanomaterial as a candidate for improving the durability of cement-based materials [23-28]. Carbon nanotubes have high flexibility, in addition to strength [29]. Titanium oxide nanoparticles also have opened a new chapter in nanotechnology research in recent years, due to their self-cleaning properties, excellent hydrophilicity, non-toxicity, abundance, and availability [30-32]. Nano-montmorillonite is one of the main nano-clay phases, and several structural properties of the clays have better reactivity and the ability to return to the initial dimensions in the vicinity of heat and flame retardation. This nanomaterial, as a modified natural substance, has achieved nanotechnology applications in nanocomposites and because of its high nature value, it can enter the industry at a lower cost than other nanomaterials [33-37]. In the above study, carbon nanotubes and titanium oxide nanoparticles were first synthesized and the dielectric properties of the powdery nanocomposites made from these materials and the montmorillonite nanoparticles and Portland cement were evaluated. Then, by design of experiments (DOE) by response surface methodology (RSM) concept, nanomaterials replaced cement in the cement paste by weight percentages. mechanical properties of the specimens were evaluated according to ASTM standards and through analyzing data, figures and spectra obtained from X-ray diffraction (XRD) and X-powder techniques, the effect of using nanomaterial in cement and its role in modifying the nanostructured properties of cement matrix were investigated.

EXPERIMENTAL PROGRAM AND SAMPLE PREPARATION

The design and method of this experimental study were approved by the nanophysics Research Center of the Faculty of Basic Sciences at the Mazandaran University.

Materials

Type II Portland cement produced in Mazandaran Cement Company was employed in the present study complying with ASTM C150, 2004 [38]. Chemical properties of the cement used in quality controlling of the cement company's laboratory were studied with XRF analysis and are presented in Table 1. and Sodium dodecyl benzene sulfonate (SDBS) as a surfactant has also been used as a nanomaterial disperser.

Synthesis of MWCNT

To synthesize carbon nanotube by CVD technique, argon gas (for 15 minutes) was injected with a flow of 300 sccm into a quartz chamber

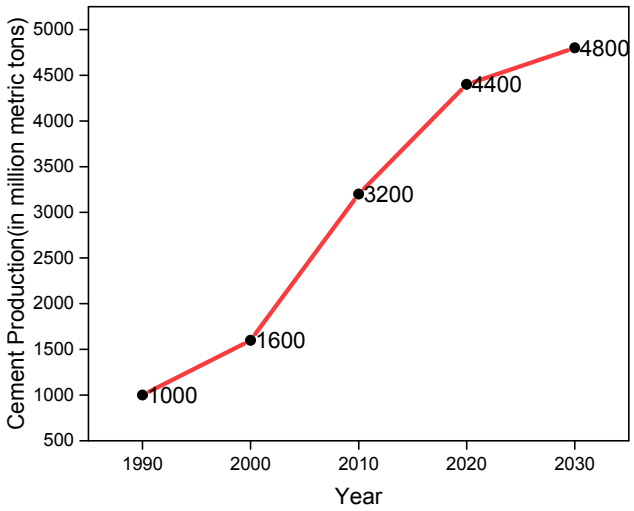

Fig. 1. Global cement production versus year, extracted from Mendes literature [2].

Table 1. Chemical compositions of PC obtained by using XRF analysis (% by weight).

	SiO_2	Al_2O_3	Fe_2O_3	CaO	MgO	SO_3	Na_2O	K_2O	C_3S	C_2S	C_3A	LOI
PC	21.32	5.13	4.08	62.45	2.11	1.98	0.41	0.63	45.57	23.79	6.55	1.45

PC: Portland cement; LOI: loss on ignition

containing 100 mg of catalyst substrate. Then, the flow of argon gas was reduced to 100 sccm and acetylene gas was released with a specific flux inside the quartz tube. In this way, the prepared substrate is placed adjacent to acetylene and argon gases. It takes about 15 minutes to complete the process of growing carbon nanotubes, dissolve the acetylene gas flow and let the material cool to room temperature in the vicinity of the argon gas (to prevent oxidation of the carbon nanotube).

Functionalization of MWCNT

For the production of operating carbon nanotubes, 5 g of synthesized carbon nanotubes were added to 200 ml of HNO_3 nitric acid solution and were diluted for 140 hours at 140° C. The material was washed with distilled water. Then solid separation from the liquid was performed by the use of centrifuge (3000 rpm). The solid products were completely dried at 60 ℃ to produce the resulting material as a MWCNT-COOH.

TEM analysis of nanomaterials

TEM analysis was used to describe the morphology and distribution of the size of carbon nanotubes and nanoparticles. The TEM image of the functionalized carbon nanotubes is shown in Fig. 2. The average outside diameter of the nanotubes is 15 to 35 nm. Montmorillonite nanoparticles were produced in Southern Clay Products, Inc. The TEM image of the nano-montmorillonite is shown in Fig. 3. The average length of the montmorillonite nanoparticles is 6 to 16 nm. Silicon carbide (β, 99%) was purchased from UD Research Nanomaterials, Inc. Titanium Oxide Nanoparticle (TiO_2, anatase) was purchased from Nanosony Corporation, Inc. The TEM image of the nano-TiO_2 is shown in Fig. 4. The average length of the TiO_2 nanoparticles

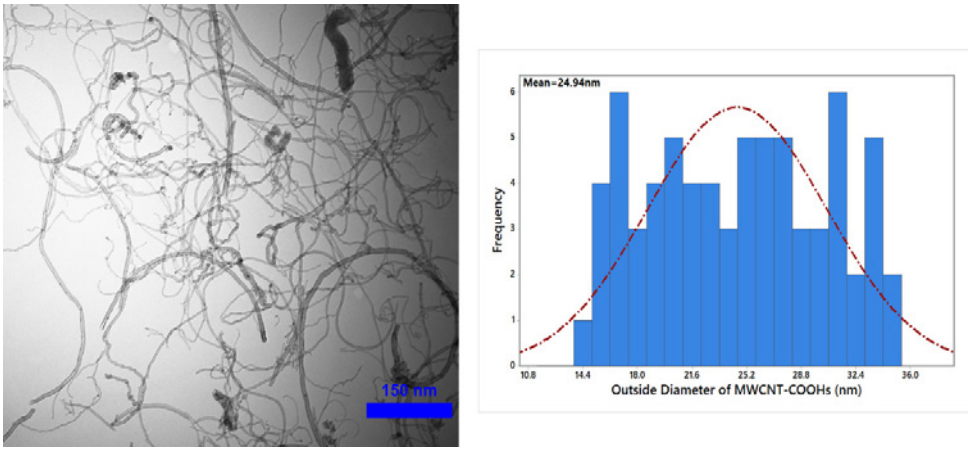

Fig. 2. TEM image and histogram of the outside diameter of the MWCNT-COOH.

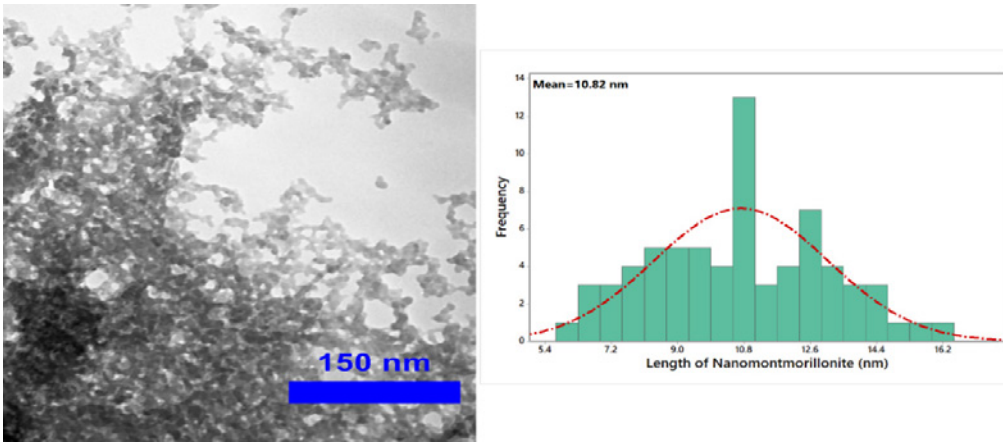

Fig. 3. TEM image and histogram of the length of montmorillonite nanoparticles.

is 18 to 45 nm. Physical properties of MWCNT-COOHs synthesized in the mentioned project can be observed in Table 2.

Preparation of cement paste samples

In the present work, five series of mixed cement paste including control samples as samples without nanomaterials and other samples containing CNT, TiO_2 and NM nanoparticles with the weight percentage of Portland cement were used according to Table 3.

The cement paste samples were prepared according to ASTM C109, 2002 [39] standard with the water to binder i.e. cement + MWCNT + NM or cement+ MWCNT + TiO_2 ratio of 0.425. For better dispersion of nanomaterials in the cement matrix, MWCNT was dispersed in deionized water using a magnetic stirrer before adding cement to make a suspension. After that, cement was added and the mixture was dispersed in water in an ultrasonic bath (BANDELIN, Germany) for 30 minutes at 25 °C for more uniform dispersion. Then, the mixture was blended by the use of a mechanical blender (TESTING Bluhm, Germany). The applied mixer for this experiment was in accordance with ASTM C511, 2013 [40] with a planetary motion of 285 rpm for paste. During the test, the laboratory temperature was 20 ± 2 °C. The samples were demolded 24 hours after they were cast and then cured in a water basin at 23 ± 2 ° C for 27 days.

Table 2. Physical properties of MWCNT-COOH.

Property	Value
Purity	>95%
Outside Diameter	15-35 nm
Inside Diameter	8-5nm
Length	≈ 50μm
Color	Black
True density	2.1 (g/cm^3)
Electrical Conductivity	100 s/cm
Manufacturing Method	CVD

Test methods

Mechanical tests

Flexural and compressive strengths of the samples were studied in 28 days. Compressive strength was done on samples based on ASTM C109, 2002 [39] standard. For this purpose, 5 cubic specimens (50×50×50 mm3) were prepared. Flexural strength tests were done on samples based on the ASTM C348, 2002 [41] standard. In this regard, 5 prismatic samples (160×40×40 mm3) were prepared. The mechanical tests were done by a cement testing machine (DIGICON, Swiss) with a capacity of 200KN and a loading speed of 2.4 KN/s for compressive strength and with a capacity of 10KN and a loading speed of 0.5 KN/s for flexural strength.

Results of mechanical tests

Table 4 shows the results of the flexural and compressive strengths of the cement paste samples at different ages with different weight ratio nanomaterials. Results of variations in compressive and flexural strengths of pure cement composites (CS) and nanocomposites containing different nanomaterials with different weight percentages shown in Fig. 5 and Fig. 6 demonstrated that the compressive and flexural strength of samples containing nanomaterials is significantly improved compared to the control sample. The highest increase in compressive strength is related to the

Table 3. Mixture designs of cement paste.

Mixture	Mix protection					
	Cement (g)	NM(g)	TiO_2(g)	CNTs(g)	SDBS(g)	Water(cc)
CS	400.00	0	0	0	0	170
SNCS1	397.52	2.4	0	0.08	0.016	170
SNCS2	398.80	0.8	0	0.40	0.080	170
STCS1	395.92	0	4	0.08	0.016	170
STCS2	393.60	0	6	0.40	0.040	170

CS: Control sample. [b]SNCS: Sample of NM+CNT+SDBS, [c]STCS: Sample of TiO2+CNT+SDBS

Table 4. Results of compressive and flexural strength (MPa).

Mixture	Compressive strength(MPa)	Flexural strength(MPa)
CS	31.87±0.016	7.75±0.004
SNCS1	39.69±0.020	10.78±0.005
SNCS2	41.36±0.020	10.68±0.005
STCS1	39.42±0.019	9.50±0.005
STCS2	38.33±0.018	9.20±0.005

SNCS2 sample and the highest increase in flexural strength is related to the SNCS1 sample.

The compressive strength of the SNCS2 sample increased by about 30%, and the flexural strength of the SNCS1 sample increased by 39% compared to the control sample. It is clear that montmorillonite nanoparticles play the greatest role in improving the mechanical properties of cement composites,

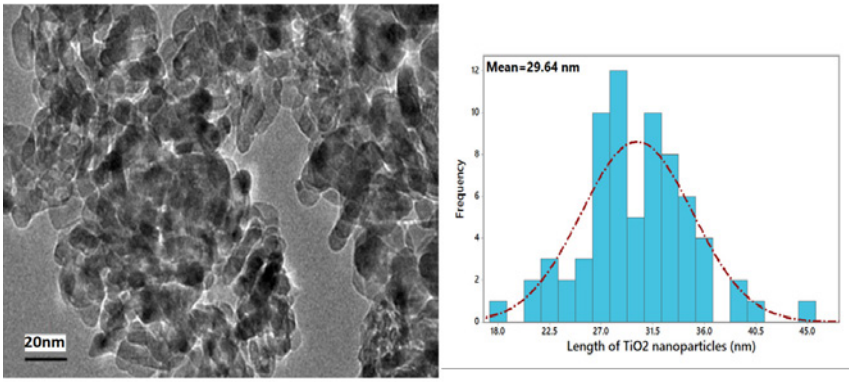

Fig. 4. TEM image and histogram of the length of TiO_2 nanoparticles.

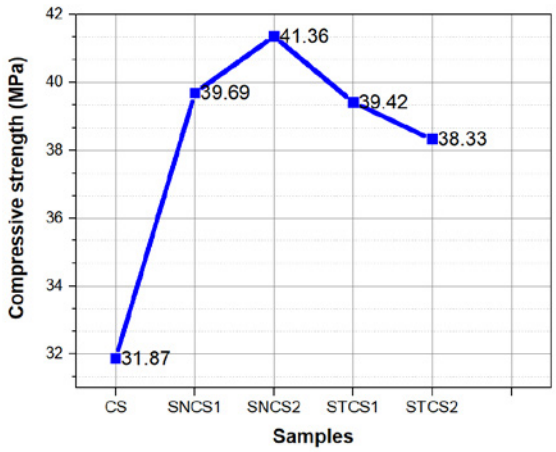

Fig. 5. Variations in compressive strength of cement-based composite.

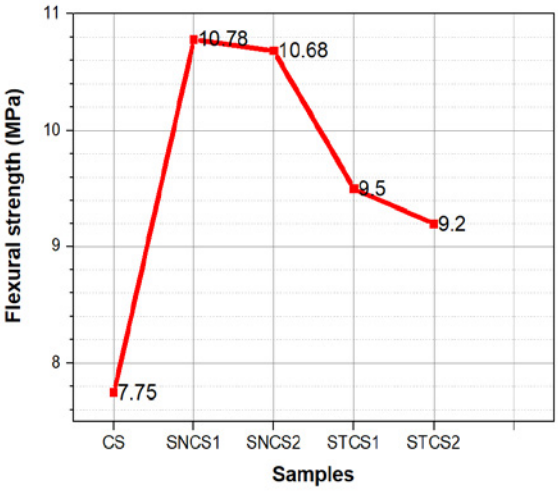

Fig. 6. Variations in flexural strength of the cement-based composite.

which can be attributed to specific surfaces and high reactivity of this nanoparticle. Another reason to improve the mechanical properties of cement-based nanocomposites is to increase the reactivity of cement products with the presence of montmorillonite and titanium dioxide nanoparticles. It means that with high surfaces and fast reactivity, the nanomaterials react with $Ca(OH)_2$ and produce a secondary gel which is the main factor in increasing the strength of cement-based nanocomposites. Another reason for the improvement of the mechanical properties of nanomaterial samples in comparison with the control samples is the presence of functionalized carbon nanotubes with the COOH group in the hydration process. The COOH function acts as a bridge between the polar hydrophilic cement matrix and non-polar carbon nanotubes, and it makes nanotubes better dispersed in the cement matrix. Furthermore, functionalized carbon nanotubes penetrate well inside cement products and by bridging, they help to reinforce interfaces. As a result, they improve the flexural strength of cementitious nanocomposite. Also, the presence of carbon nanotubes in the hydration process causes a delay in its duration, and more C-S-H is produced. Improvement of the mechanical properties of nanocomposites can also be due to the filling property of nanoparticles. Due to their very small dimensions, nanoparticles penetrate into cementitious pores as filler and fill the empty spaces and cause more cementitious cavitation and thus improve mechanical properties. In order to prevent agglomeration and produce better dispersion in the cementitious matrix, the SDBS surfactant and also the ultrasonic bath is used in the process of making nanocomposites.

MICROSTRUCTURE ANALYSIS

To confirm the mechanical test results in the previous section, the microstructure analysis of samples containing nanomaterials was compared with the control sample using the following methods.

XRD analysis and X-Powder technique

The XRD method can be used to determine phase identification, crystal size measurement, and crystallinity. The phases of the powdery samples, without and with nanomaterials were qualitatively and quantitatively analyzed by XRPD [W: 1200, 35: KV, 30: mA] with a tube FK 60-04, cobalt anode, and linear focus, and the data were collected as follows: Time per step: 1 sec; angular range: 5-80°; total acquisition time: 01:23 h; degrees/min: ½.

Fig. 7 shows the XRD patterns of pure cement paste (CS) and cement nanocomposites containing CNTs, TiO_2 nanoparticles (STCS1 and STCS2) and CNTs, NM nanoparticles (SNCS1 and SNCS2). According to the figure, the peaks located at 47.1°, 34.2°, 18.2°, and 8.50° correspond to $Ca(OH)_2$, where the intensity of SNCS2 and STCS1 decreased compared to CS, whereas the peak intensity at 29.5° , related to C-S-H, increased in samples containing nanomaterials, especially in the SNCS2 sample. The peak at 34° is related to the C-H bond, and its

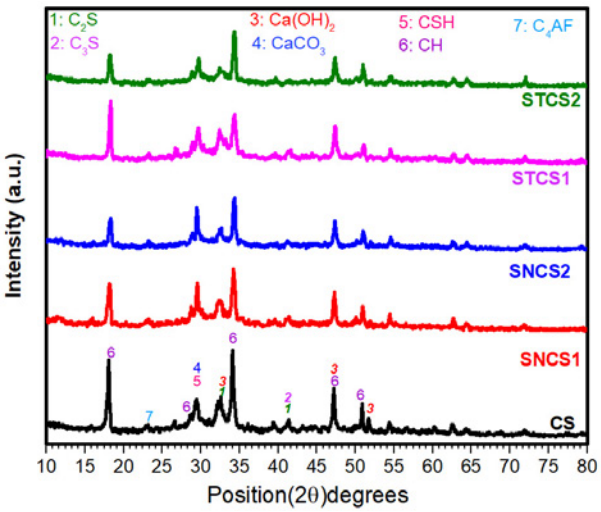

Fig. 7. XRD patterns of the control sample (CS) and reinforced cement paste samples at the ages of 3 and 28 days.

intensity has decreased in nanocomposite samples compared to CS. Also, peaks of 41.3° and 32.5° are related to the presence of C_2S and C_3S, which is reduced in samples containing nanomaterials, particularly SNCS2, compared to CS. All of these findings indicate improved nanostructured properties of cement-based nanocomposites that are consistent with mechanical test results. In addition, by reducing the structure of amorphous in cement composites, the electrical resistance of cement-based nanocomposites decreases.

The data were quantitatively analyzed by the Scherrer method using the X-Powder software. In order to measure the approximate sizes of the crystal phases, the width of the peak was measured at half the maximum intensity (FWHM) and the highest-intensity peak was chosen. Based on Scherrer's model according to Eq. 1 [42]:

$$D = \frac{0.9\lambda}{\beta cos\theta} \quad (1)$$

D is the crystal size, β is the peak width at half the maximum intensity, θ is the Bragg angle related to the peak, and λ is the X-ray wavelength. Based on the equation, as the peak width increased, the crystal size decreased as a result of the addition of nanomaterials in cement paste. As shown in Fig. 8, the size of the nano-crystallites in the CS is 61

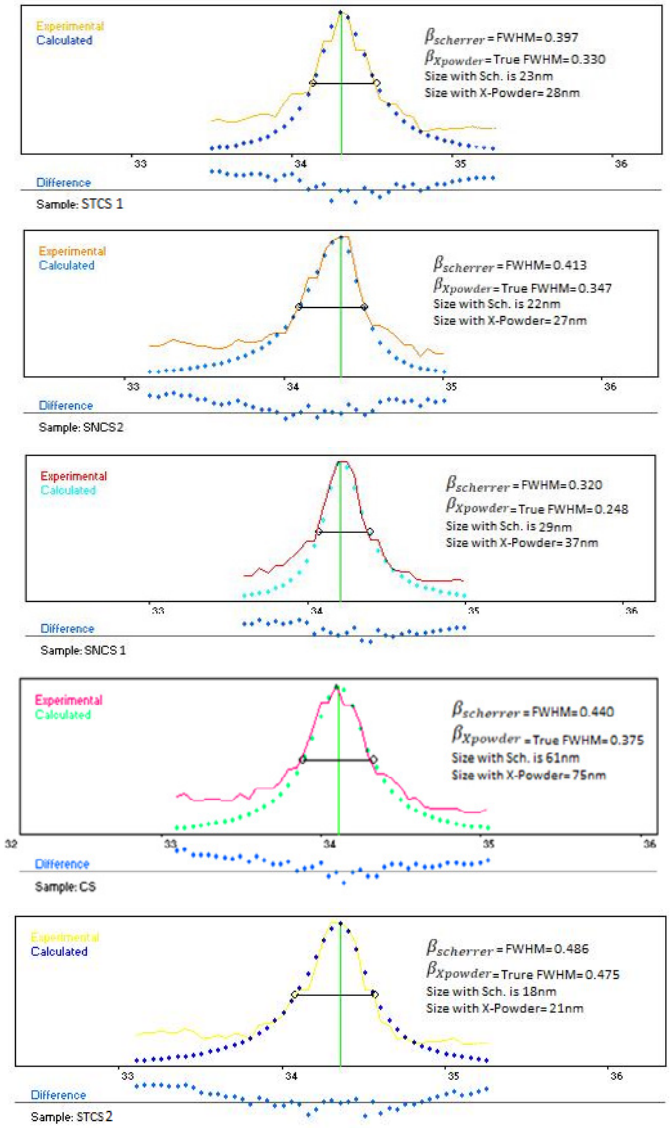

Fig. 8. Size of nanocrystallite for the control sample, cement paste containing nano-TiO_2, NM particles and MWCNT-COOH calculated with the Scherrer equation and X-powder technique.

nm and 75 nm, in the SNCS1 sample, it is 29 nm and 37 nm, in the SNCS2 sample, 22 nm and 27 nm, in the STCS1 sample, 23 nm and 38 nm, and in STCS2 sample, it is 18nm, and 21 nm, which was obtained using both Sherer relation and the X-Powder technique.

FTIR properties

To determine the quantitative and qualitative properties of cement paste containing nanomaterials, type of the functional group and the bonds in their molecules can be determined using the FTIR spectrophotometric method. Fig. 9 illustrates the chemical bond between the samples containing nanomaterials and CS in a range of 400-4000 cm^{-1}. Fig. 9 shows the FTIR spectra of the control sample and cement-based nanocomposites containing different nanomaterials. The peak in the range of wave number 450 to 463 Cm^{-1} corresponds to the SiO(υ_4) functional group [43,44]. This peak in the sample without nanomaterials is in 462 Cm^{-1} and in the samples containing carbon nanotubes, montmorillonite nanoparticles and, titanium oxide nanoparticles (SNCS1, SNCS2, STCS1 and STCS2) in the wave number 459 Cm^{-1} shows more intensity. Due to the inverse relationship between the wave number and the displacement energy toward the lower wave number, it can be attributed to the stronger bond energy. The peak in the range of the wave number 874 to 878 Cm^{-1} corresponds to the CO_3^{-2} (υ_4) bond [43] and the peak of samples containing nanomaterials is smaller than the control sample. In the range of 968 to 971Cm^{-1}, it is related to stretch vibration for SiO(υ_3) functional group [45-47] which is no significant change between samples containing nanomaterials and the control sample.

Considering the fact that the existing peak in the range of wavenumber 1426 to 1430 Cm^{-1} is related to the functional group CO_3^{-2} (υ_3)[48,49], peak in the wavenumber 1426 Cm^{-1} for the control sample and with changes fully reduced in the wavenumber 1420 Cm^{-1}, it is observed that the bonding related to CO_3^{-2} (υ_3) is a little weaker. In the wavenumber range of 1640 to 1650 Cm^{-1}, the peak related to the functional group is $H_2O(\upsilon_2)$ [47-50] where the target peak for the CS, the SNCS1 and SNCS2 is observed in the wavenumber 1641 Cm^{-1} and for the STCS1 and STCS2, it is observed in the wavenumber 1652 Cm^{-1}. Also in the samples containing nanomaterials, the peaks are observed as intensified. The peaks in the range of wavenumber 3399 to 3444 Cm^{-1} corresponded to the functional group O-H(υ_3) [51] which is observed in wavenumber 3438 Cm^{-1} and the changes related to the samples containing nanomaterials compared to the CS are not observable. In the range of wavenumber 3641 to 3644 Cm^{-1} the peak is corresponded to calcium hydroxide $Ca(OH)_2$ [50]. This peak for every five samples is observed in the wavenumber 3642 Cm^{-1} and this peak is more intensive in the samples containing nanomaterials.

QUALITY AND EMISSION FACTORS OF THE SAMPLES

As stated before, the cement industry produces large amounts of CO_2. It is under pressure to reduce both greenhouse gas emissions and energy. For this

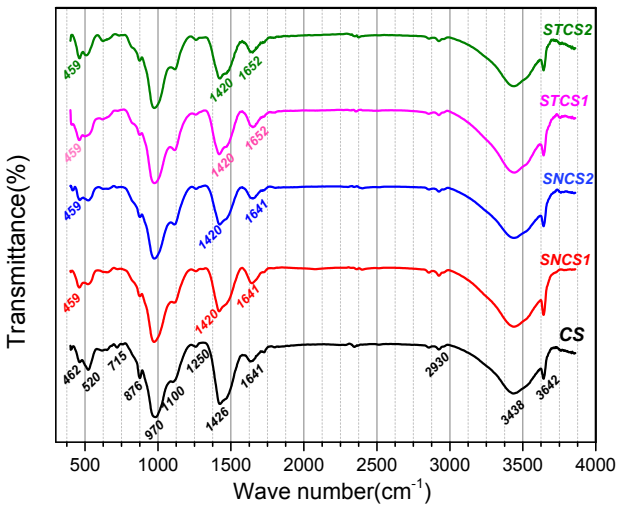

Fig. 9. FTIR spectra of the control sample (CS) and reinforced cement paste samples

purpose, the quality factor (Q_F) and dissipation factor (D_F) is studied where five capacitors were constructed. The capacity of the samples was measured by the use of GPS 132 A. Then dielectric constant (k) is calculated using the equation $c=k\varepsilon_0$ A/d. In the constructed tables: r=1.2 cm, d=2mm and $\varepsilon_{0=8.85\times10^{-12}}\left(\frac{C^2}{Nm^2}\right)$.

Results in Tables 5 and 6 show that capacity (C), dielectric constant (k), quality factor (Q_F), and

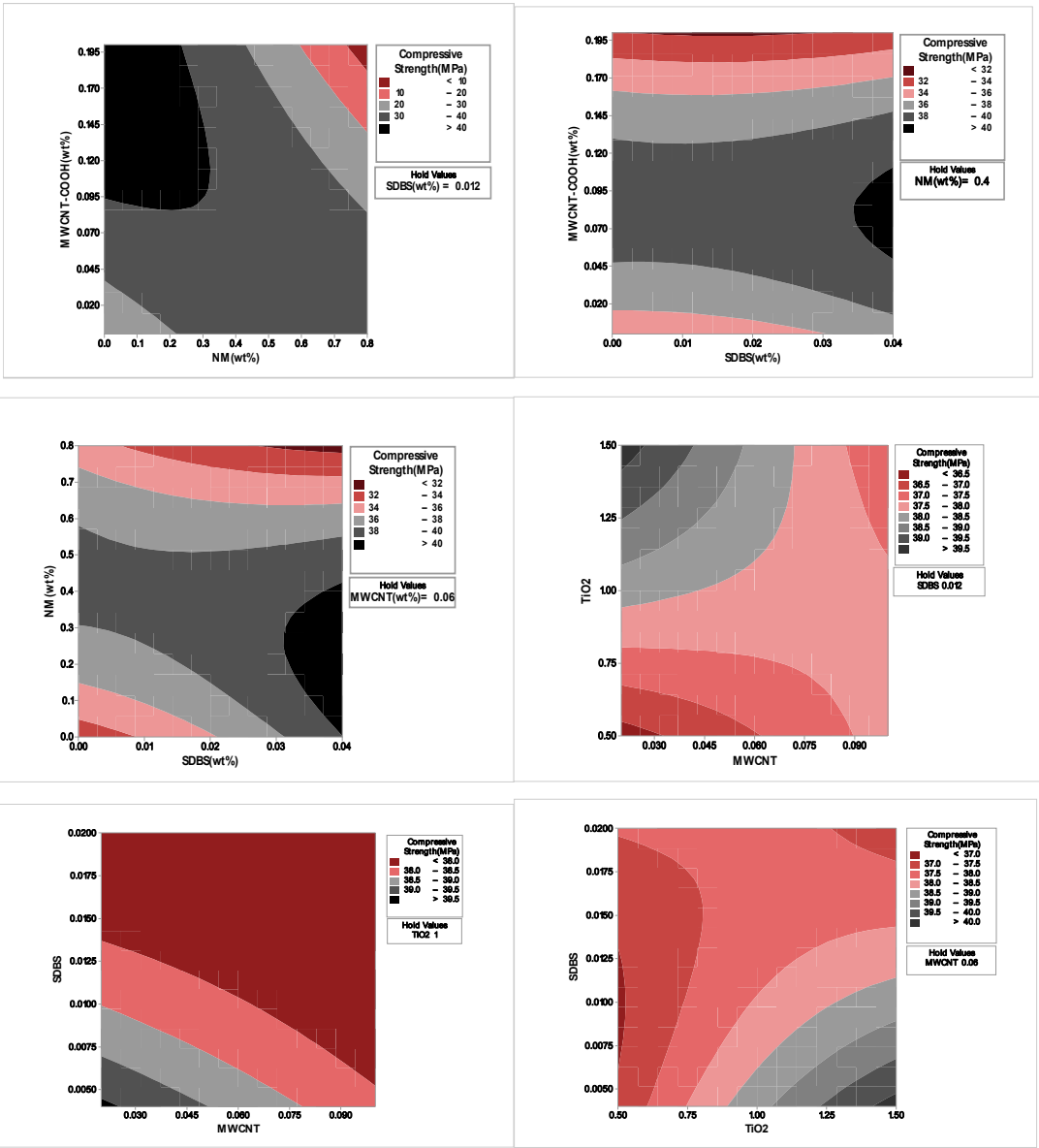

Fig. 10. Contour plots of compressive strengths versus nanomaterial interactions

Table 5. Q_F, D_F, C and k of nanocomposites obtained by using GPS 132 A (f = 120 Hz)

Sample	Q_F	D_F	C (pF)	k
CS	3.85	0.259	1902.31	8.00
SNCS1	25.37	0.040	250.76	21.05
STCS1	19.16	0.052	75	5.11
SNCS2	33.24	0.030	425	38.12
STCS2	13.71	0.073	358	4.01

Table 6. Q_F, D_F, C and k of nanocomposites are obtained by using GPS 132 A (f = 1 KHz)

Sample	Q_F	D_F	C (pF)	k
CS	3.85	0.259	1902.31	8.00
SNCS1	25.37	0.040	250.76	21.05
STCS1	19.16	0.052	75	5.11
SNCS2	33.24	0.030	425	38.12
STCS2	13.71	0.073	358	4.01

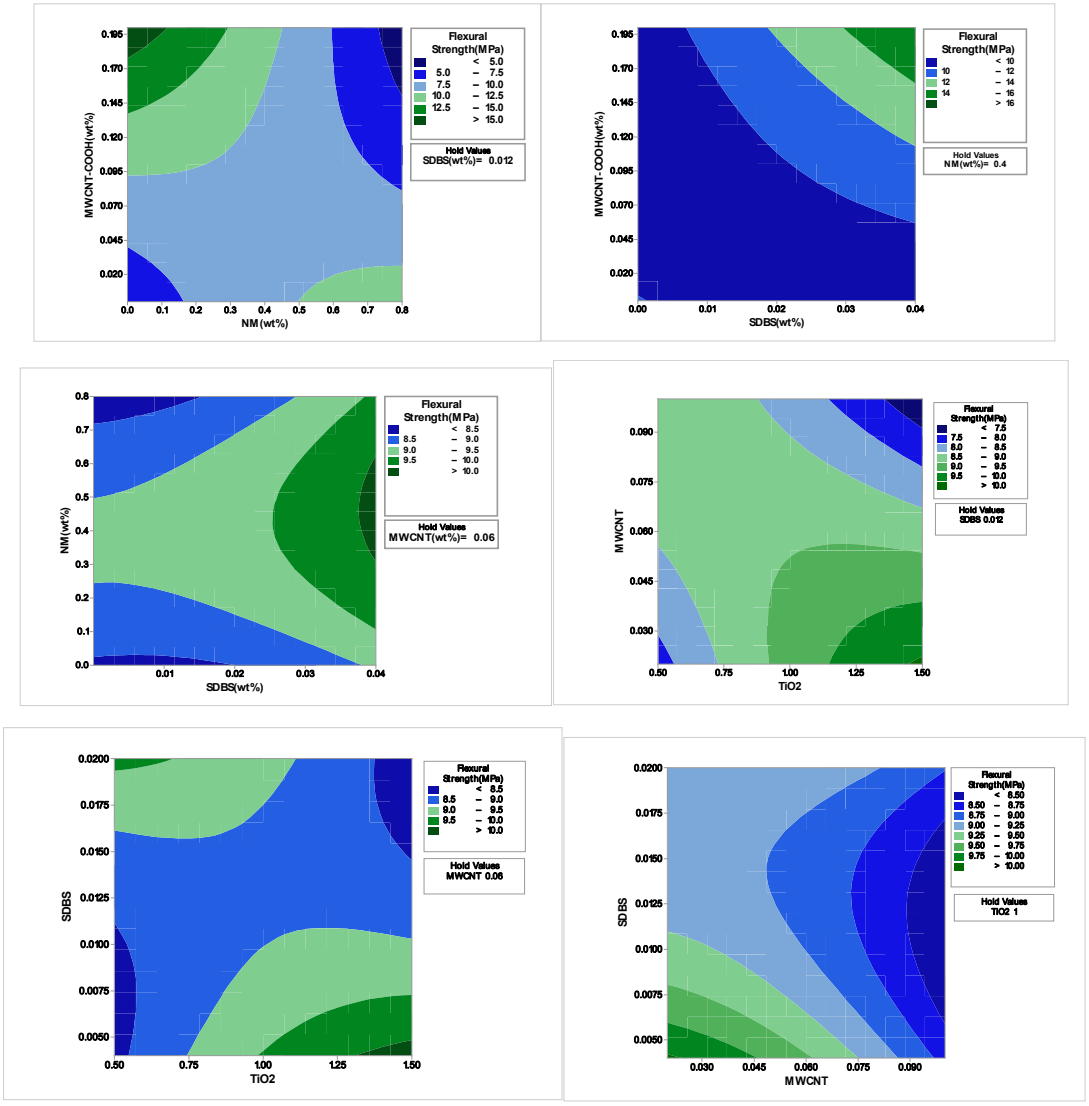

Fig. 11. Contour plots of flexural strengths versus nanomaterial interactions

dissipation factor (D_F) change after adding different powdery materials to CNTs. The maximum amounts of dielectric constant at the frequency of 120 Hz (38.12) and 1 kHz (17.02) are related to SNCS2 sample. The maximum value of Q_F represents the minimum energy loss rate regarding the energy stored in the capacitor, which is obtained through the Eq. (2):

$$Q_F = 2 \frac{\text{Energy stored}}{\text{energy dissipated per cycle}} \quad (2)$$

The D_F value is obtained from Eq. 3 which expresses the energy loss rate of the capacitor and varies with different dielectric materials, as presented in Tables 5 and 6.

$$D_F = \frac{1}{Q_F} \quad (3)$$

The estimated fraction emission factor, f in Eq. 4 and according to XRD patterns in Figs. 7 and 8 for samples in Tables 5 and 6 at 120 Hz for CS, SNCS1, STCS1, SNCS2 and STCS2 is about 0.875, 0.684,0.746, 0.612, and 0.743 respectively.

$$E_{cement} = f_{Cement}^{CaO} \frac{M_r^{CO_2}}{M_r^{CaO}} \quad (4)$$

Where E_{cement} the emission factor, f is is the fraction of CaO in cement, $M_r^{CO_2}$ and M_r^{CaO} are the molecular weight of CO_2 (44.01) and the molecular weight of CaO (56.08) respectively [55]. It is clear that E_{SNCS2} has lower emission factor than the other present samples.

DESIGN OF EXPERIMENT BY RSM CONCEPT

In this study, the design of experiments was used to save time and money, and the results of the mechanical test section are the best results of this design. Design of experiment (DOE) is a systematic process to analyze the test and to optimize input variables levels to get optimum value for output response. Response surface methodology (RSM) is an important issue in the statistical design of experiment which is a complex of useful arithmetic and statistical techniques for molding and is a response variable that determines the relationship between one or more response variables and several independent inputs. The aim is to optimize this response.

One of the objectives of using RSM is to understand the topography of the response surface (local maximum, local minimum, ridge lines) and finding the regions where the optimal response occurs. RSM is an iterative process by which experiments are conducted along the pathway of steepest ascent (i.e. the direction of greatest improvement in the response variable) in order to identify the factor settings which optimize the response variable. The response changes in a given direction by adjusting the design variables. Using two-dimensional plots from the experimental design software, optimal concentrations of nanomaterials replaced in cement paste were predicted to achieve the highest results of mechanical tests as responses. The plots are helpful to see the shape of a response surface. The function $y = f(x_1, x_2, x_3)$ can be plotted versus the levels of (x_1, x_2), (x_2, x_3) and (x_1, x_3). In this graph, each value of x_1, x_2 and x_3 generates a *y*-value.

The contour plots show contour lines of (x_1, x_2), (x_2, x_3) and (x_1, x_3) pairs that have the same response value y. In this study, the contour plots illustrate contour lines of (NM, CNTs), (NM, SDBS), (CNTs, SDBS), (TiO_2, CNTs), (TiO_2, SDBS) and (CNTs, SDBS) pairs that have the compressive and flexural strengths as responses in Figs. 10 and 11. Using two-dimensional contour plots, we estimated the optimal concentrations of carbon nanotubes, titanium oxide, montmorillonite nanoparticles and SDBS in pairs which resulted in the highest compressive and flexural strengths.

CONCLUSION

In the present theoretical and empirical study, carbon nanotubes were synthesized and functionalized, and after the design of experiment, some nanoparticles (TiO_2, MWCNT, and NM) replaced cement in the cement matrix. The best results of mechanical tests have been reported. Then, the nano-structural factor, as well as quality and emission factors, were studied. The obtained results indicated that sample SNCS2 with higher dielectric constant (38.12), higher quality factor (33.24) and lower emission factor (0.612) is a suitable sample in the cement-based industry.

CONFLICT OF INTEREST

The authors declare that there are no conflicts of interest regarding the publication of this manuscript.

REFERENCES

[1] M.S. Shetty, Concrete Technology: Theory and Practice, 7th ed., S. Chand &Company PVT. Ltd., 1982.

[2] T. Mendes, D. Hotza, and W. Repette, Nanoparticles in cement based materials: A review., Rev. Adv. Master. Sci., 40 (2015) 89-96.

[3] 7th international VDZ Congress (2013), Global Cement Production From 1990 to 2030 (in million metric tons). accessed 26 February (2018).

[4] G. Eamon, Getting the Numbers Right, the Cement Sustainability Initiative, WBCSD, (2016).

5. Damineli BL, Kemeid FM, Aguiar PS, John VM. Measuring the eco-efficiency of cement use. Cement and Concrete Composites. 2010;32(8):555-62.

6. Sadeghi-Nik A, Berenjian J, Bahari A, Safaei AS, Dehestani M. Modification of microstructure and mechanical properties of cement by nanoparticles through a sustainable development approach. Construction and Building Materials. 2017;155:880-91.

7. Wei J, Meyer C. Sisal fiber-reinforced cement composite with Portland cement substitution by a combination of metakaolin and nanoclay. Journal of Materials Science. 2014;49(21):7604-19.

8. Li W, Huang Z, Cao F, Sun Z, Shah SP. Effects of nano-silica and nano-limestone on flowability and mechanical properties of ultra-high-performance concrete matrix. Construction and Building Materials. 2015;95:366-74.

9. Nazari A, Riahi S. Corrigendum to "The effect of TiO2 nanoparticles on water permeability and thermal and mechanical properties of high strength self compacting concrete" [Mater. Sci. Eng. A 528 (2010) 756–763]. Materials Science and Engineering: A. 2011;528(9):3526.

10. Zhang H, Zhao Y, Meng T, Shah SP. Surface Treatment on Recycled Coarse Aggregates with Nanomaterials. Journal of Materials in Civil Engineering. 2016;28(2):04015094.

11. Kong Y, Wang P, Liu S, Gao Z, Rao M. Effect of microwave curing on the hydration properties of cement-based material containing glass powder. Construction and Building Materials. 2018;158:563-73.

12. Siddique R, Schutter Gd, Noumowe A. Effect of used-foundry sand on the mechanical properties of concrete. Construction and Building Materials. 2009;23(2):976-80.

13. Khan MI, Siddique R. Utilization of silica fume in concrete: Review of durability properties. Resources, Conservation

and Recycling. 2011;57:30-5.
14. Amin MS, Habib AO, Abo-El-Enein SA. Hydrothermal characteristics of high-slag cement pastes made with and without silica sand. Advances in Cement Research. 2012;24(1):23-31.
15. Hashem FS, Amin MS, El-Gamal SMA. Improvement of acid resistance of Portland cement pastes using rice husk ash and cement kiln dust as additives. Journal of Thermal Analysis and Calorimetry. 2012;111(2):1391-8.
16. El-Gamal SMA, El-Hosiny FI, Amin MS, Sayed DG. Ceramic waste as an efficient material for enhancing the fire resistance and mechanical properties of hardened Portland cement pastes. Construction and Building Materials. 2017;154:1062-78.
17. Abo-El-Enein SA, Hashem FS, Amin MS, Sayed DM. Physicochemical characteristics of cementitious building materials derived from industrial solid wastes. Construction and Building Materials. 2016;126:983-90.
18. Sanchez F, Sobolev K. Nanotechnology in concrete – A review. Construction and Building Materials. 2010;24(11):2060-71.
19. Chen J, Liang C, Li B, Wang E, Li G, Hou X. The effect of nano-γAl 2 O 3 additive on early hydration of calcium aluminate cement. Construction and Building Materials. 2018;158:755-60.
20. El-Gamal SMA, Abo-El-Enein SA, El-Hosiny FI, Amin MS, Ramadan M. Thermal resistance, microstructure and mechanical properties of type I Portland cement pastes containing low-cost nanoparticles. Journal of Thermal Analysis and Calorimetry. 2017;131(2):949-68.
21. El-Gamal SMA, Hashem FS, Amin MS. Influence of carbon nanotubes, nanosilica and nanometakaolin on some morphological-mechanical properties of oil well cement pastes subjected to elevated water curing temperature and regular room air curing temperature. Construction and Building Materials. 2017;146:531-46.
22. Hamedi M, Karabulut E, Marais A, Herland A, Nyström G, Wågberg L. Nanocellulose Aerogels Functionalized by Rapid Layer-by-Layer Assembly for High Charge Storage and Beyond. Angewandte Chemie. 2013;125(46):12260-4.
23. Bahari A, Sadeghi Nik A, Roodbari M, Mirnia N. Investigation the Al–Fe–Cr–Ti nano composites structures with using XRD and AFM techniques. Sadhana. 2012;37(6):657-64.
24. Chen J, Liang C, Li B, Wang E, Li G, Hou X. The effect of nano-γAl 2 O 3 additive on early hydration of calcium aluminate cement. Construction and Building Materials. 2018;158:755-60.
25. A. Bahari, A. Sadeghi Nik, M. Roodbari, K. Taghavi, and S. E. Mirshafiei. Synthesis and strength study of cement mortars containing sic nano particles., Dig. J. Nanomater. Biostructures., 7 (2012) 1427–1435.
26. Bahari A, Berenjian J, Sadeghi-Nik A. Modification of Portland Cement with Nano SiC. Proceedings of the National Academy of Sciences, India Section A: Physical Sciences. 2016;86(3):323-31.
27. Zhang H, Guo L, Song Q, Fu Q, Li H, Li K. Microstructure and flexural properties of carbon/carbon composite with in-situ grown carbon nanotube as secondary reinforcement. Progress in Natural Science: Materials International. 2013;23(2):157-63.
28. Björnström J. Effect of superplasticizers on the rheological properties of cements. Materials and Structures. 2003;36(264):685-92.
29. Sobolev K, Ferrada Gutiérrez M. How Nanotechnology Can Change the Concrete World. Progress in Nanotechnology: John Wiley & Sons, Inc.; 2014. p. 117-20.
30. Cassar L. Photocatalysis of Cementitious Materials: Clean Buildings and Clean Air. MRS Bulletin. 2004;29(05):328-31.
31. Folli A, Pade C, Hansen TB, De Marco T, Macphee DE. TiO2 photocatalysis in cementitious systems: Insights into self-cleaning and depollution chemistry. Cement and Concrete Research. 2012;42(3):539-48.
32. Chen J, Poon C-s. Photocatalytic Cementitious Materials: Influence of the Microstructure of Cement Paste on Photocatalytic Pollution Degradation. Environmental Science & Technology. 2009;43(23):8948-52.
33. Chang T-P, Shih J-Y, Yang K-M, Hsiao T-C. Material properties of portland cement paste with nano-montmorillonite. Journal of Materials Science. 2007;42(17):7478-87.
34. Kuo W-Y, Huang J-S, Lin C-H. Effects of organo-modified montmorillonite on strengths and permeability of cement mortars. Cement and Concrete Research. 2006;36(5):886-95.
35. Sadeghi-Nik A, Berenjian J, Bahari A, Safaei AS, Dehestani M. Modification of microstructure and mechanical properties of cement by nanoparticles through a sustainable development approach. Construction and Building Materials. 2017;155:880-91.
36. Chang T-P, Shih J-Y, Yang K-M, Hsiao T-C. Material properties of portland cement paste with nano-montmorillonite. Journal of Materials Science. 2007;42(17):7478-87.
37. Kafi MA, Sadeghi-Nik A, Bahari A, Sadeghi-Nik A, Mirshafiei E. Microstructural Characterization and Mechanical Properties of Cementitious Mortar Containing Montmorillonite Nanoparticles. Journal of Materials in Civil Engineering. 2016;28(12):04016155.
38. ASTM C150-04, Standard Specification for Portland Cement, ASTM International, West Conshohocken, PA., (2004).
39. Specification for Mixing Rooms, Moist Cabinets, Moist Rooms, and Water Storage Tanks Used in the Testing of Hydraulic Cements and Concretes. ASTM International.
40. Test Method for Compressive Strength of Hydraulic Cement Mortars (Using 2-in. or [50-mm] Cube Specimens). ASTM International.
41. ASTM C348-02, Standard Test Method for Flexural Strength of Hydrauliccement Mortars, ASTM International, West Conshohocken, PA., (2002).
42. Derlet PM, Van Petegem S, Van Swygenhoven H. Calculation of x-ray spectra for nanocrystalline materials. Physical Review B. 2005;71(2).
43. Gomes CEM, Ferreira OP, Fernandes MR. Influence of vinyl acetate-versatic vinylester copolymer on the microstructural characteristics of cement pastes. Materials Research. 2005;8(1):51-6.
44. Barnett SJ, Macphee DE, Lachowski EE, Crammond NJ. XRD, EDX and IR analysis of solid solutions between thaumasite and ettringite. Cement and Concrete Research. 2002;32(5):719-30.
45. Kloprogge JT, Schuiling RD, Ding Z, Hickey L, Wharton D, Frost RL. Vibrational spectroscopic study of syngenite formed during the treatment of liquid manure with sulphuric acid. Vibrational Spectroscopy. 2002;28(2):209-21.
46. Kloprogge JT, Schuiling RD, Ding Z, Hickey L, Wharton D, Frost RL. Vibrational spectroscopic study of syngenite formed during the treatment of liquid manure with sulphuric acid. Vibrational Spectroscopy. 2002;28(2):209-21.
47. Mollah MYA, Yu W, Schennach R, Cocke DL. A Fourier

transform infrared spectroscopic investigation of the early hydration of Portland cement and the influence of sodium lignosulfonate. Cement and Concrete Research. 2000;30(2):267-73.
48. Mollah MYA, Lu F, Cocke DL. An X-ray diffraction (XRD) and Fourier transform infrared spectroscopic (FT-IR) characterization of the speciation of arsenic (V) in Portland cement type-V. Science of The Total Environment. 1998;224(1-3):57-68.
49. Trezza MA, Lavat AE. Analysis of the system 3CaO·Al2O3–CaSO4·2H2O–CaCO3–H2O by FT-IR spectroscopy. Cement and Concrete Research. 2001;31(6):869-72.
50. Ylmén R, Jäglid U, Steenari B-M, Panas I. Early hydration and setting of Portland cement monitored by IR, SEM and Vicat techniques. Cement and Concrete Research. 2009;39(5):433-9.
51. Silva DA, Roman HR, Gleize PJP. Evidences of chemical interaction between EVA and hydrating Portland cement. Cement and Concrete Research. 2002;32(9):1383-90.
52. Hall EO. The Deformation and Ageing of Mild Steel: III Discussion of Results. Proceedings of the Physical Society Section B. 1951;64(9):747-53.
53. Hansen N. Hall–Petch relation and boundary strengthening. Scripta Materialia. 2004;51(8):801-6.
54. Nieh TG, Wadsworth J. Hall-petch relation in nanocrystalline solids. Scripta Metallurgica et Materialia. 1991;25(4):955-8.
55. Andrew RM. Global CO2 emissions from cement production, 1928–2017. Earth System Science Data. 2018;10(4):2213-39.